High-Gain Dual-Circularly Polarized Leaky-Wave Antenna for Point-to-Point Communications

Ye, Qi-Cheng; Zhang, Yiming; Li, Jia-Lin; Zhang, Shuai

Published in:
I E E E Antennas and Wireless Propagation Letters

Publication date:
2022

Document Version
Accepted author manuscript, peer reviewed version

High-Gain Dual-Circularly Polarized Leaky-Wave Antenna for Point-to-Point Communications

Qi-Cheng Ye, *Member, IEEE*, Yi-Ming Zhang, *Member, IEEE*, Jia-Lin Li, Ming Yao, *Student Member, IEEE*, and Shuai Zhang, *Senior Member, IEEE*

***Abstract*—In this work, a high-gain low-profile dual circularly polarized (CP) leaky-wave antenna (LWA) with fixed beam is presented. The proposed LWA comprises only two-layered substrates, in which the top layer constructs the annular LWA array while the bottom layer realizes the feeding network. To obtain the fixed beam, the differential excitation generated by the proposed coupler is employed. Further, the dual CP feeding network provides two sequentially rotated phase excitations for the slot coupler, then the dual CP radiation with fixed beam is realized. The profile height of the proposal is only $0.15\lambda_0$ at 28 GHz, while the measured peak gain is up to 27.2 dBic; this could be attractive for point-to-point communications.**

***Index Terms*—High gain, dual-circularly polarized antenna, leaky-wave antenna (LWA), low profile, point-to-point communications.**

I. Introduction

As the development of communication technology, the point-to-point wireless backhaul links have to provide ultrahigh data rate, large capacity, and low latency. The millimeter-wave (mm-wave) technique is an attractive scheme [1]. Meanwhile, forceful directivity is also required for the mm-wave antenna due to the encountered propagation loss, especially for the long-distance scene [2]. It is well known that circularly polarized (CP) wave is conducive to communication quality enhancement due to polarization insensitivity and anti-multipath interference [3]. Compared to the single CP, the dual CP antenna can further improve system agility since it can realize two polarization states.

Recently, many techniques have been developed for dual CP mm-wave antennas. In [4] and [5], by using the 3-dB coupler, a pair of orthogonal excitations with ±90° phase difference is obtained to excite the whole array. The delay line method can also gain the 90° phase difference between the orthogonal excitation signals [6]. Moreover, the array using sequentially rotated (SR) phase excitation with two rotation directions can also achieve dual CP radiation [7], [8]. By further introducing the Berry phase based on the excitation phase, an SR array with a single-port feed can generate dual beams with different CP handedness [9], [10]. Besides these schemes, the septum polarizer is an often-used method to realize dual CP radiation, including the element and array design [11], [12]. Several dual CP multibeam antennas using septum polarizers are also reported [13], [14]. In the dual CP horn designs, except for the septum polarizer [15], the mono-groove polarizer is also used [16]. For the transmitarrays [17], [18] and reflectarrays [19], [20], using the CP feeding horn or polarizer to obtain the dual CP is a typical method.

On the other hand, several mm-wave leaky-wave antennas (LWA) with single CP [21], [22], or dual CP radiation have been reported [23], [24]. In [23], the curved microstrip line is served as the CP element, and the dual CP radiation is reached by exciting the opposite feeding ports. The design in [24] is to use a 3-dB coupler to obtain a ±90° phase difference within the orthogonal two-element array. Please note that the beams of these LWAs are scanning versus frequencies. To the best knowledge of the authors, there are few studies on the CP LWA features the fixed beam. In our previous work [25], by employing the differential feed, a dual linearly polarized (LP) LWA with fixed beam is presented.

To facilitate the development of CP-wave point-to-point communications, a high-gain dual CP LWA with fixed beam and low profile is proposed. In this letter, the radiation mechanism concerning the fixed beam is first investigated. Then, the annular LWA unit cell and the customized coupler to realize CP radiation is presented and analyzed. A miniaturized dual SR CP feeding network is further developed for dual CP operation. The proposed design is fabricated and measured for verification purposes.

II. Antenna Design and Analysis

The proposed dual CP antenna is composed of two-layered substrates, as presented in Fig. 1, in which the top layer is the radiation layer, and the bottom layer is the feeding layer. The used substrates are Rogers RO3003, with a dielectric constant of 3.0 and a thickness of 0.762 mm. For the radiation layer, seven periods of annular LWA unit cells are etched on the top surface, while the boundary is sealed off with 0.15mm radius metallized vias. The substrate integrated waveguide (SIW) technique constructs the feeding network. The inputted signals from the feeding layer are coupled to the radiation layer

Manuscript received ×××; revised ×××; accepted ×××. Date of publication ×××; date of current version ×××. *(Corresponding author: Shuai Zhang.)*

Qi-Cheng Ye is with the School of Physics, University of Electronic Science and Technology of China, Chengdu 611731, China, and also with the Antenna, Propagation and Millimeter-wave Systems (APMS) Section, Aalborg University, 9220 Aalborg, Denmark (e-mail: qichengye@std.uestc.edu.cn).

Yi-Ming Zhang is with the Guangdong Provincial Key Laboratory of Optoelectronic Information Processing Chips and Systems, School of Electronics and Information Technology, Sun Yat-Sen University, Guangzhou 510006, China (email: zhangyim9@mail.sysu.edu.cn)

Jia-Lin Li is with the School of Resources and Environment, University of Electronic Science and Technology of China, Chengdu 611731, China (e-mail: jialinli@uestc.edu.cn).

Ming Yao and Shuai Zhang are with the Antenna, Propagation and Millimeter-wave Systems (APMS) Section, Aalborg University, 9220 Aalborg, Denmark (e-mail: mingya@es.aau.dk; sz@es.aau.dk).

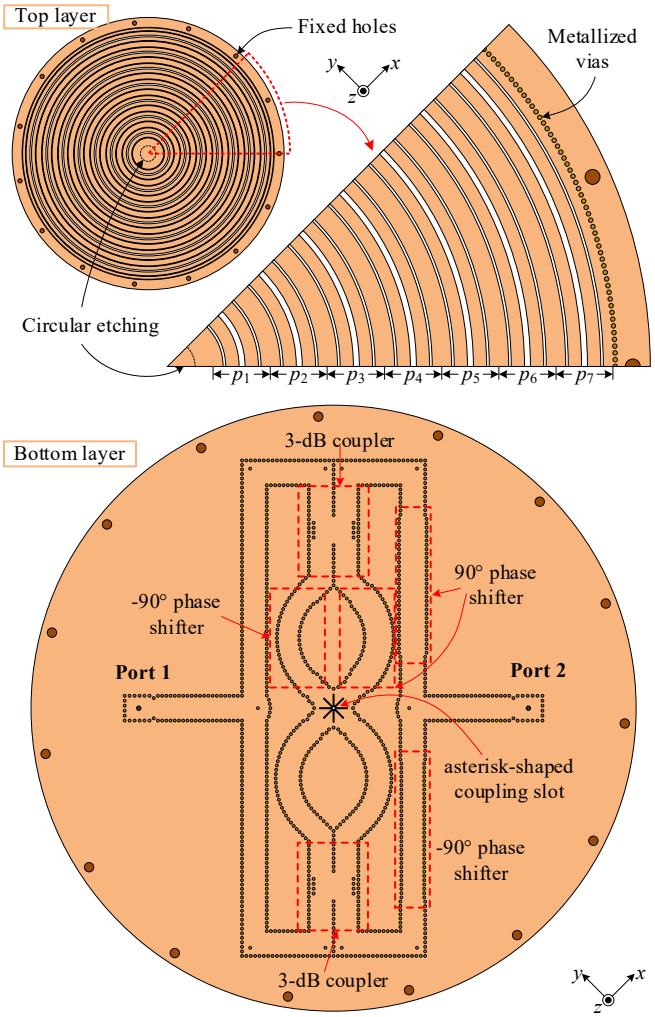

Fig. 1. Configuration of the proposed dual CP antenna.

through the central asterisk-shaped slot. The full-wave electromagnetic (EM) simulations are performed by CST 2019.

A. Radiation Mechanism

The simplified radiation mechanism diagrams (top view and section view) are presented in Fig. 2, where the original asterisk-shaped slot is diminished as a single rectangular slot to ease the analysis. As shown in Fig. 2(a), when the E-fields perpendicular to the slot is excited in the slot, the quasi-TEM mode waves are generated and propagated along the radial direction of the parallel plate waveguide (PPW). Notably, the waves on both sides of the rectangular slot (Parts A and B) are out of phase, as seen in Fig. 2(b). In this way, the particular propagation mode facilitates the fixed-beam generation of LWA is obtained, i.e., the converse propagation directions and the 180° phase difference [25]. Next, through the well-designed LWA unit cells with open stopband suppression, the EM waves can be radiated to synthesize the fixed beam.

The annular slots composing the LWA unit cell are ideal for cutting the arched surface currents and radiating the scanning beam. Since the dominant power is excited perpendicular to

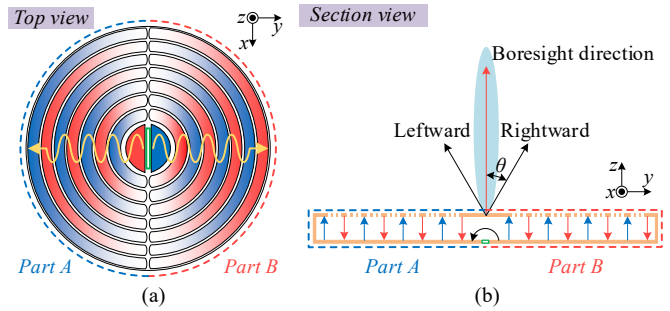

Fig. 2. Radiation mechanism of the proposed antenna. (a) Top view. (b) Section view. (Green rectangle denotes the coupling slot)

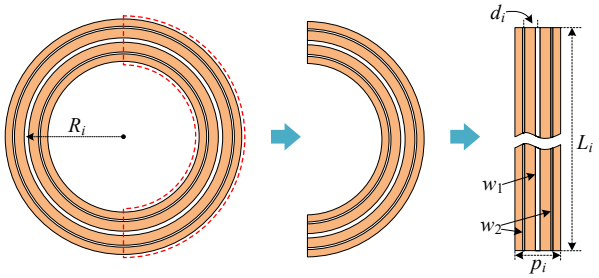

Fig. 3. Fundamental annular unit cell and the transformed straight model.

the rectangular slot (see the darker color in Fig. 2(a)), it can be expected that the equivalent co-polarized orientations of LP scanning beams radiated by Parts A and B are perpendicular to the slot. Meanwhile, due to the particular propagation mode, the polarization orientations of the two scanning beams are identical at any moment. According to the study in [25], when two co-polarized scanning beams are approached by each other within a small angular space of $2\times\theta$, a fixed beam in boresight direction can always be synthesized. Further, to enhance the radiation efficiency, the edge of the PPW is closed with metallized vias to make partial unit cells operate in standing-wave mode. Due to the edged conductor boundary providing the antiphase, the polarization orientations of the reflected waves are the same as the forward waves. Compared to [25], the center feed effectively reduces the overall size of the antenna by removing the peripheral transition components.

B. Annular LWA Unit Cell

Different from the conventional LWA, the unit cell in this design features an annular shape, as shown in Fig. 3. It has been proved that this unit cell with three unequal-width slots can suppress the open stopband and operate in the standing-wave mode [25]. Due to the symmetrical propagation mode, the annular unit cell can be simplified as half one and further analyzed by the straight model. In the initial few periods near the rectangular slot, since the guided wavelength slightly becomes shorter as the radius increases, the phase constant β and attenuation constant α will be variated if the uniform unit cells are used as usual. To realize the single beam direction, β for all unit cells should be the same, according to (1) [26], where k_0 is the free-space wavenumber.

$$\theta \approx \sin^{-1}\left(\frac{\beta}{k_0}\right) \tag{1}$$

For this purpose, firstly, the i_{th} unit cell length L_i is set as

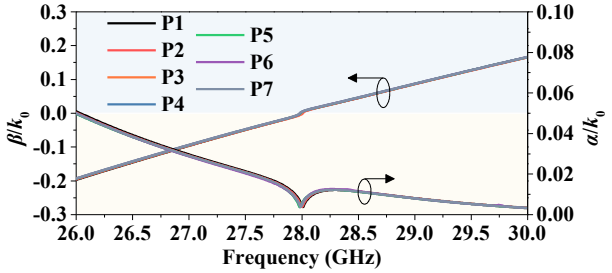

Fig. 4. Normalized phase and attenuation constants for the optimized periods.

the same as arc length in the modeling; it can be written as:

$$L_i = \pi \cdot R_i = \pi \cdot (R_{i-1} + p_{i-1}/2 + p_i/2) \quad (2)$$

where R_1 is preferably set as 10 mm. By accurately modeling the lengths of unit cells, α and β for periods at different radii can be precisely obtained with simulation. Next, by optimizing the unit cell width p and slot spacing d for initial few periods (the widths of two slots kept unchanged), the same β for all unit cells are involved (optimum parameters: w_1=0.4 mm, w_2=0.13 mm, p_1=7.69 mm, p_2=7.66 mm, p_3 to p_7 are all 7.65 mm, d_1=2.37 mm, d_2 to d_7 are all 2.35 mm). The normalized α and β are given in Fig. 4 and seeing that all the normalized α and β are almost identical to each other.

C. Implementation of CP Radiation

By analyzing the case with a single rectangular slot, the implementation mechanism of the LP fixed beam is explained well. To obtain the CP fixed beam, the polarization orientation of the LP beam needs to rotate along the beam center in sequence. A high-efficient arbitrarily-orientation differential coupler (AODC) is designed for this purpose, as shown in Fig. 5(a). It consists of two pairs of orthogonal differential channels, an asterisk-shaped coupling slot, and PPW. By exciting four inputted ports using SR phases, i.e., 0°, 90°, 180°, and 270°, the vortical wave pattern used to produce LHCP radiation can be inspired in PPW through the coupling slot, as seen in Fig. 5(b). The converse SR phases realize RHCP radiation. The wave patterns excited by initial designs are also presented as a comparison. It is found that the proposed AODC exhibits a more uniform pattern than others since the asterisk-shaped slot can couple the waves from multiple orientations. In fact, the uniform amplitude and good phase continuity can realize high CP purity. Fig. 5(c) gives the reflection coefficients and the coupling efficiency (received power by perfectly matched layer / inputted power) of the proposed AODC. It is observed that the active reflection coefficients are lower than −22 dB within 26 to 30 GHz, while the coupling efficiency is higher than 97%. Besides the CP excitation, the proposed AODC can also realize LP excitation patterns, e.g., vertical, horizontal, and diagonal polarization.

III. Design of Feeding Network

To supply the SR phases for AODC, a feeding network based on the SIW technique is designed, as shown in Fig. 1. Different from the usual designs with a single SR phase, the proposed network provides two kinds of SR phases, i.e., clockwise and counterclockwise, to realize dual CP radiation.

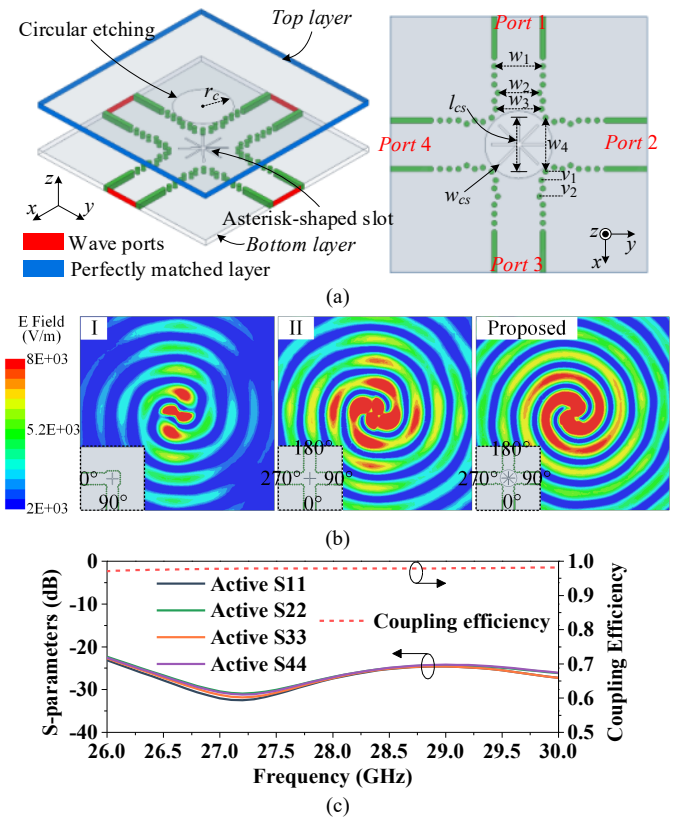

Fig. 5. (a) Configuration of the proposed coupler. (b) Excitation wave patterns for three kinds of coupler. (c) Active S parameters and coupling efficiency of the proposed AODC. (l_{cs}=5.98 mm, w_{cs}=0.22 mm, r_c=3.7 mm, w_1=5.3 mm, w_2=4.54 mm, w_3=4.99 mm, w_4=5.88 mm, v_1=0.96 mm, v_2=1.77 mm.)

As seen, the whole configuration consists of 3-dB couplers, ±90° phase shifters, and power dividers. The SIW-based inputted ports using the probe excitation. The used 3-dB couplers and phase shifters in Fig. 6 are carefully designed for this network, then the good amplitude imbalance of less than 1.6 dB and phase imbalance of less than 13.9° for four outputted ports is realized from 27 to 29 GHz. Meanwhile, the isolation between two inputted ports is higher than 34 dB. Compared to the network in [7], the improved configuration and arrangement in this design achieve a more compact layout.

IV. Experiments and Comparisons

The fabricated dual CP antenna and measuring scene are shown in Fig. 7, where two substrates are fixed on the metal base via plastic screws. Moreover, two MMPX connectors are used to connect the feeding network and the measuring device.

Fig. 8(a) shows the simulated and measured S parameters of the proposed antenna. It is seen that the simulated and measured reflection coefficients for both two ports are lower than −13 dB from 27 to 29 GHz. For the isolation between two ports, the simulated result is higher than 10 dB within 27.05 to 28.75 GHz, while the measured one is larger than 27 dB. Since the feeding network provides high isolation, the leaked power must reflect by the conductor boundary in the radiation layer to reach the isolated port. The contrary phase and propagation direction contributed by the conductor boundary allow the leaked power to be received by the isolated port. For

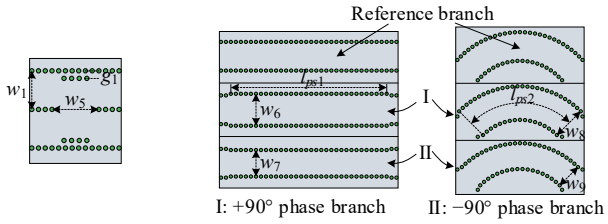

Fig. 6. (a) 3-dB coupler. (b) ±90° phase shifters for straight type and bent type. (w_5=6.45 mm, g_1=1.04 mm, l_{ps1}=28.6 mm, w_6=5.9 mm, w_7=4.9 mm, l_{ps2}=19.93 mm, w_8=6.2 mm, w_9=4.76 mm.)

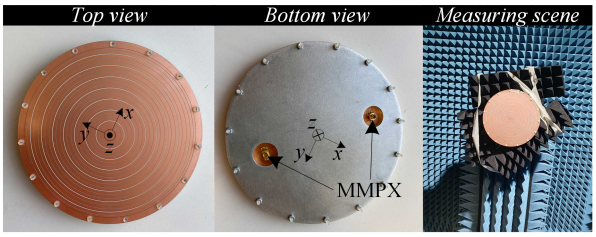

Fig. 7. Fabricated antenna protype and measuring scene.

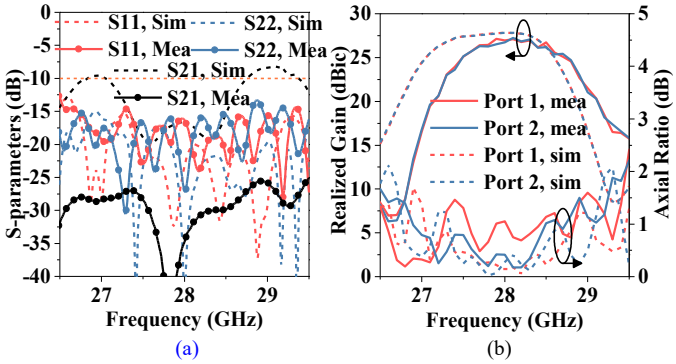

Fig. 8. Simulated and measured performance for the proposed dual CP antenna. (a) Reflection coefficient and isolation. (b) Gain and AR.

such a long path, a higher practical path loss causing that the measured isolation is higher than the simulation. The 3-dB AR and gain performances in boresight direction are presented in Fig. 8(b). As seen, the simulated and measured AR values are less than 3 dB over the whole operating band, both for two CP states. For the measured gain, it is higher than 23.6 dBic from 27.4 to 28.8 GHz (5% relative bandwidth). Due to the phase constant shift resulting from manufacturing error in unit cells, the measured gain curves are slightly shifted about 0.3 GHz to the high frequencies compared to the simulations. The far-field radiation patterns in *xoz*-plane at 27.5, 28, and 28.5 GHz are illustrated in Fig. 9, and seeing that the simulated and measured patterns are in good agreement. The slight difference between the simulated and measured co-polarized sidelobe levels is observed as the shifted phase constants affect the synthesized beam patterns. Note that the cross-polarized beams at around ±7° are caused by the arrangement of the array itself. Since the CP wave is formed by two orthogonal LP fields with 90° phase difference, the array generates strong sidelobes with phase reversal in one of the fields, making the total fields there form the cross-polarized beams. The communications that rely on the high-gain beam are unaffected as they are always far from the main beam.

The comparisons between this work and other reported dual

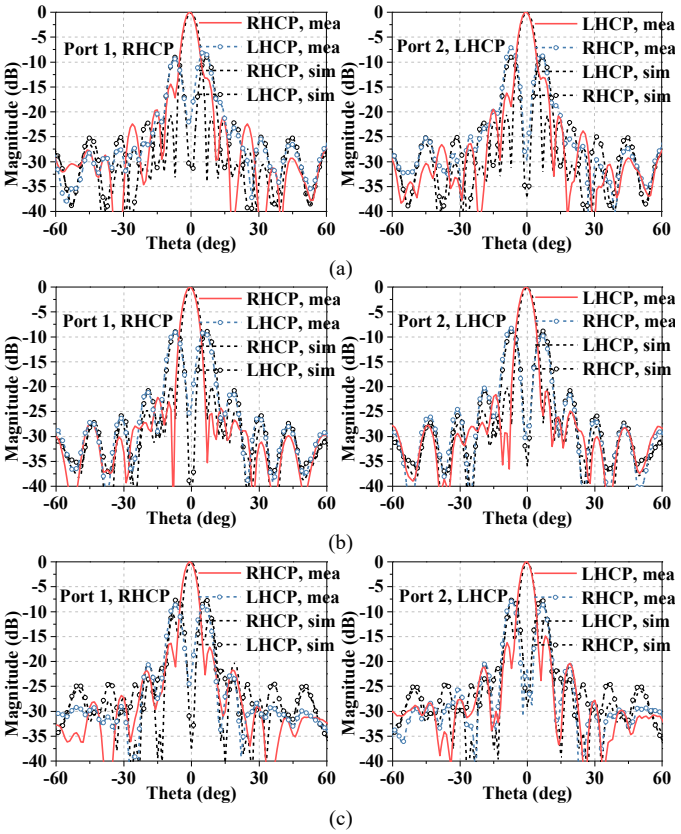

Fig. 9. Simulated and measured radiation patterns of the proposed antenna. (a) 27.5 GHz. (b) 28 GHz. (c) 28.5 GHz.

TABLE I
COMPARISONS BETWEEN THIS WORK AND REPORTED DUAL CP ANTENNAS

Ref.	Freq. (GHz)	Antenna Type	Operating Bandwidth	Aperture Efficiency	Max Gain (dBic)	Total Profile
[6]	60	Patch	23%	64.1%	25.8	$0.7\lambda_0$
[7]	60	Strip and cavity	17%	28%	17.85	$0.16\lambda_0$
[12]	30	Waveguide array	16%	95.6%	32.8	$5.06\lambda_0$
[17]	29	Transmitarray	7.3%	36.6%	31.4	$14.24\lambda_0$
[20]	30	Reflectarray	14.7%*	28%	28.4	$14.6\lambda_0$
This work	28	LWA	5%	42.4%	27.2	$0.15\lambda_0$

* denotes 1-dB gain and AR < 2 dB bandwidth.

CP designs are listed in Table I. Due to the particular beam synthesis mechanism, the relative operating bandwidth of this work with available gains and radiation patterns is lower than the others. Nevertheless, this work exhibits a comprehensive advantage in profile height, gain, and aperture efficiency. Although the total profile for [7] is similar to this work, the gain and the aperture efficiency are much lower, while the profiles for other designs are clearly higher than this work.

V. CONCLUSION

A high-gain low-profile dual CP LWA with fixed beam is presented in this letter. To realize the dual CP radiation, the annular LWA unit cell, the customized coupler, and the dual SR phase feeding network are employed. The measured results show that the operating band ranges from 27.4 to 28.8 GHz, and the maximum gain is up to 27.2 dBic. The profile height of only $0.15\lambda_0$ (at 28 GHz) could be attractive for compact point-to-point communications.

REFERENCES

[1] A. Vosoogh, M. S. Sorkherizi, V. Vassilev, A. U. Zaman, Z. S. He, J. Yang, A. A. Kishk, and H. Zirath, "Compact integrated full-duplex gap waveguide-based radio front end for multi-Gbit/s point-to-point backhaul links at E-band," *IEEE Trans. Microw. Theory Techn.*, vol. 67, no. 9, pp. 3783–3797, Sep. 2019.

[2] D. Lockie and D. Peck, "High-data-rate millimeter-wave radios," *IEEE Microw. Mag.*, vol. 10, no. 5, pp. 75–83, Aug. 2009.

[3] S. Gao, Q. Luo, and F. Zhu, *Circularly Polarized Antennas*. Hoboken, NJ, USA: Wiley, 2014.

[4] Y. J. Cheng, J. Wang, and X. L. Liu, "94 GHz substrate integrated waveguide dual-circular-polarization shared-aperture parallel-plate long-slot array antenna with low sidelobe level," *IEEE Trans. Antennas Propag.*, vol. 65, no. 11, pp. 5855-5861, Nov. 2017.

[5] M. Ferrando-Rocher, J. I. Herranz-Herruzo, A. Valero-Nogueira, and B. Bernardo-Clemente, "Dual circularly polarized aperture array antenna in gap waveguide for high-effificiency Ka-band satellite communications," *IEEE Open J. Antennas Propag.*, vol. 1, pp. 283–289, 2020.

[6] Y. Zhao and K.-M. Luk, "Dual circular-polarized SIW-fed high-gain scalable antenna array for 60 GHz applications," *IEEE Trans. Antennas Propag.*, vol. 66, no. 3, pp. 1288–1298, Mar. 2018.

[7] J. Zhu, S. Liao, Y. Yang, S. Li, and Q. Xue, "60 GHz dual-circularly polarized planar aperture antenna and array," *IEEE Trans. Antennas Propag.*, vol. 66, no. 2, pp. 1014–1019, Feb. 2018.

[8] P. F. Kou and Y. J. Cheng, "A dual circular-polarized extremely thin monopulse feeder at W-band for prime focus reflector antenna," *IEEE Antennas Wireless Propag. Lett.*, vol. 18, no. 2, pp. 231–235, Feb. 2019.

[9] R. F. Ma, Z. H. Jiang, Y. Zhang, X. Y. Wu, T. Yue, W. Hong, and D. H. Werner, "Theory, design, and verification of dual-circularly polarized dual-beam arrays with independent control of polarization: A generalization of sequential rotation arrays," *IEEE Trans. Antennas Propag.*, vol. 69, no. 3, pp. 1369-1382, Mar. 2021.

[10] X. Y. Wu, Z. H. Jiang, Y. Zhang, T. Yue, W. Hong, and D. H. Werner, "Generalized sequential rotation arrays with full control of dual-circularly-polarized aperture-field distribution based on elliptically-polarized elements," *IEEE Trans. Antennas Propag.*, (Early Access) doi: 10.1109/TAP.2022.3177489.

[11] X. Cheng, Y. Yao, T. Yu, J. Yu, and X. Chen, "Wideband dual circularly polarized antipodal septum antenna for millimeter-wave applications," *IEEE Trans. Antennas Propag.*, vol. 69, no. 6, pp. 3549-3554, Jun. 2021.

[12] J. Wu, Y. J. Cheng, H. B. Wang, Y. C. Zhong, D. Ma, and Y. Fan, "A wideband dual circularly polarized full-corporate waveguide array antenna fed by triple-resonant cavities," *IEEE Trans. Antennas Propag.*, vol. 65, no. 4, pp. 2135–2139, Apr. 2017.

[13] C. Wang, J. Wu, and Y.-X. Guo, "A 3-D-printed multibeam dual circularly polarized Luneburg lens antenna based on quasi-icosahedron models for Ka-band wireless applications," *IEEE Trans. Antennas Propag.*, vol. 68, no. 8, pp. 5807–5815, Aug. 2020.

[14] M. Farahani, M. Akbari, M. Nedil, A.-R. Sebak, and T. A. Denidni, "Millimeter-wave dual left/right-hand circularly polarized beamforming network," *IEEE Trans. Antennas Propag.*, vol. 68, no. 8, pp. 6118–6127, Aug. 2020.

[15] C. Shu, J. Wang, S. Hu, Y. Yao, J. Yu, Y. Alfadhl, and X. Chen, "A wideband dual-circular-polarization horn antenna for mmWave wireless communications," *IEEE Antennas Wireless Propag. Lett.*, vol. 18, no. 9, pp. 1726-1730, Sep. 2019.

[16] N. Luo, X. Yu, G. Mishra, and S. K. Sharma, "A millimeter-wave (V-band) dual-circular-polarized horn antenna based on an inbuilt monogroove polarizer," *IEEE Antennas Wireless Propag. Lett.*, vol. 19, no. 11, pp. 1933-1937, Nov. 2020.

[17] K. T. Pham, A. Clemente, D. Blanco, and R. Sauleau, "Dual-circularly polarized high-gain transmitarray antennas at Ka-band," *IEEE Trans. Antennas Propag.*, vol. 68, no. 10, pp. 7223-7227, Oct. 2020.

[18] P. Naseri, S. A. Matos, J. R. Costa, C. A. Fernandes, and N. J. G. Fonseca, "Dual-band dual-linear-to-circular polarization converter in transmission mode application to K/Ka-band satellite communications," *IEEE Trans. Antennas Propag.*, vol. 66, no. 12, pp. 7128–7137, Dec. 2018.

[19] P. Xu, L. Li, R. Li, and H. Liu, "Dual-circularly polarized spin-decoupled reflectarray with FSS-back for independent operating at Ku-/Ka-bands," *IEEE Trans. Antennas Propag.*, vol. 69, no. 10, pp. 7041-7046, Oct. 2021.

[20] Z. H. Jiang, T. Yue, and W. Hong, "Low-profile and wideband dual-circularly polarized reflect-arrays based on rotated metal-backed dual-polarized aperture-coupled patch elements," *IEEE Trans. Antennas Propag.*, vol. 68, no. 3, pp. 2108–2117, Mar. 2020.

[21] A. Zandamela, A. Al-Bassam, and D. Heberling, "Circularly polarized periodic leaky-wave antenna based on dielectric image line for millimeter-wave radar applications," *IEEE Antennas Wireless Propag. Lett.*, vol. 20, no. 6, pp. 938-942, Jun. 2021.

[22] G. Mishra, S. K. Sharma, and J. S. Chieh, "A high gain series-fed circularly polarized traveling-wave antenna at W-band using a new butterfly radiating element," *IEEE Trans. Antennas Propag.*, vol. 68, no. 12, pp. 7947–7957, Dec. 2020.

[23] Y.-H. Yang, B.-H. Sun, and J.-L. Guo, "A low-cost, single-layer, dual circularly polarized antenna for millimeter-wave applications," *IEEE Antennas Wireless Propag. Lett.*, vol. 18, no. 4, pp. 651–655, Apr. 2019.

[24] Y. J. Cheng, W. Hong, and K. Wu, "Millimeter-wave half mode substrate integrated waveguide frequency scanning antenna with quadri-polarization," *IEEE Trans. Antennas Propag.*, vol. 58, no. 6, pp. 1848–1855, Jun. 2010.

[25] Q.-C. Ye, Y.-M. Zhang, J.-L. Li, G. F. Pedersen, and S. Zhang, "High-isolation dual-polarized leaky-wave antenna with fixed beam for full-duplex millimeter-wave applications," *IEEE Trans. Antennas Propag.*, vol. 69, no. 11, pp. 7202-7212, Nov. 2021.

[26] A. A. Oliner, and D. R. Jackson, "Leaky-Wave Antenna" in *Antenna Engineering Handbook*, 4th ed., J. Volakis, Ed. New York: McGraw-Hill, 2007.